Colloids and Surfaces A: Physicochemical and Engineering Aspects 664 (2023) 131136

Contents lists available at ScienceDirect

Colloids and Surfaces A: Physicochemical and Engineering Aspects

journal homepage: www.elsevier.com/locate/colsurfa

Formation mechanism of surface modified iron oxide nanoparticles using controlled hydrolysis reaction in supercritical CO_2

Yasuhiko Orita *, Keito Kariya, Thossaporn Wijakmatee, Yusuke Shimoyama

Department of Chemical Science and Engineering, Tokyo Institute of Technology, 2-12-1 S1-33, Ookayama, Meguro-ku, Tokyo 152-8550, Japan

HIGHLIGHTS

- Oleic acid-modified iron oxide NPs is synthesized in supercritical CO_2.
- Smaller amount of water allows the formation of densely and chemically modified NPs.
- Larger amount of water leads to the formation of aggregated NPs.
- The formation of iron oleate complexes is validated by FT-IR analysis.
- Formation mechanism is discussed by experimental results and predicted solubility.

GRAPHICAL ABSTRACT

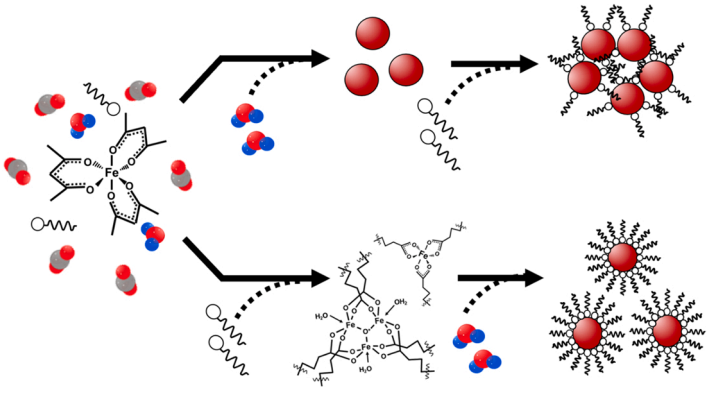

ARTICLE INFO

Keywords:
Supercritical carbon dioxide
Iron oxide nanoparticles
Surface modification
Hydrolysis reaction

ABSTRACT

In the synthesis of surface modified nanoparticles (NPs), supercritical CO_2 is one of appealing reaction fields to realize simple and green chemistry approach without using an organic solvent. In this work, surface modified iron oxide NPs was synthesized in supercritical CO_2 with various amounts of water between 5.0 and 90.0 mmol to elucidate the formation mechanism of surface modified NPs with the hydrolysis reaction. The synthesis was performed at 30.0 ± 0.9 MPa of CO_2, 18 h and 100 °C, where iron(III) acetylacetonate, water and oleic acid were used as starting materials. As a result, the smaller amount of water was revealed to be key factor to synthesize more densely modified iron oxide NPs without the aggregation and iron oxyhydroxide formation while the larger amount of water caused the sever aggregation of less modified NPs and the formation of iron oxyhydroxide. Additionally, the detailed analysis of iron oleate complex and the phase state prediction suggested that the smaller amount of water allowed more dominated formation of iron oleate and subsequent its hydrolysis reaction in uniform supercritical CO_2 phase, resulting in the formation of densely modified NPs without the aggregation.

* Corresponding author.
E-mail address: orita.y.aa@m.titech.ac.jp (Y. Orita).

https://doi.org/10.1016/j.colsurfa.2023.131136
Received 16 December 2022; Received in revised form 27 January 2023; Accepted 10 February 2023
Available online 14 February 2023

1. Introduction

Surface modified metal oxide nanoparticles (NPs) have attracted major attention during the last few decades due to their appealing properties [1]. Surface modification reduces the surface energy of NPs and induces the strong steric repulsion force between NPs, improving their dispersibility to solvent and allowing the some practical application such as thin film fabrication [2], patterning on the substrate [3] and drug delivery system [4]. Especially, the one-pot synthetic system of surface modified NPs can prevent the aggregation in the reaction field and can control their size and shape that significantly affects the physicochemical properties [5,6].

Various methods have been applied to the direct synthesis of surface modified NPs such as sol-gel [7], hot-injection [8], heat-up [9] and hydrothermal methods [10]. These wet-based methods can control the size, shape and surface property of the NPs, however, these methods typically cause the large amount of waste liquor for the synthesis and washing [5,9,10], where the disposal and regeneration cost of them is known as the major problem. Whereas the synthesis in supercritical carbon dioxide ($scCO_2$) can be one of the appealing candidates to synthesize surface modified NPs because $scCO_2$ can be used as not only synthesis but also washing and drying solvent for the particle production [11,12], which enables the simple fabrication process without using a solvent. Additionally, $scCO_2$ has high solubility of metal organic precursor and high diffusivity, which allows the formation of uniform reaction field [13]. These merits have promoted the synthesis research using $scCO_2$ for inorganic materials such as metal oxide [14], metal hydroxide [11] and metal sulfate [15]. However, the products have been frequently observed as aggregates after the synthesis in $scCO_2$ [14,16], which is probably due to the non-polar property of CO_2 that has low compatibility with the hydrophilic surface of metal oxide.

Introduction of organic surfactant to the synthesis in $scCO_2$ could modify the surface of metal oxide particles, which effectively changes their surface property from hydrophilic to hydrophobic that is compatible with CO_2 [17,18]. Additionally, the surface modification can also induce strong steric repulsion force between particles [5,19]. Furthermore, $scCO_2$ has high solubility of organic surfactant that is typically used for the synthesis of surface modified NPs such as saturated and unsaturated fatty acids [20,21]. These expectation and potential of $scCO_2$ have promoted our recent study about the direct synthesis of surface modified NPs using $scCO_2$ as a reaction field. As a result, we successfully synthesized chemically and densely modified iron oxide NPs using water and surfactant in $scCO_2$ [22]. Additionally, the hydrolysis reaction in $scCO_2$ was suggested to be the key role to synthesize NPs. However, the effect of water amount on the crystal structure, morphology and surface property of obtained NPs should be clarified to control their properties. In this study, surface modified iron oxide NPs was synthesized in $scCO_2$ with various amounts of water to understand its effect on the characteristic of obtained NPs and to elucidate the formation mechanism with the hydrolysis reaction.

Iron oxide NPs are the excellent biocompatible material approved by the US Food and Drug Administration for use in humans [23] and have appealing magnetic properties such as strong magnetic saturation and superparamagnetism [24], which allows many biomedical applications [25–27]. Especially in use as contrast agent, their superparamagnetic property (below about 20 nm) allows more emphasized magnetic resonance imaging [27]. In use as drug carrier, iron oxide NPs allow the long blood circulation time in human body due to their small size [28] and can be magnetically guided to the target site due to their strong magnetic saturation [24]. For these applications, hydrophobically modified iron oxide NPs are typically used as the starting material [9,29,30], and their surface state are transformed into hydrophilic via the ligand exchange reaction [29] and polymer coating [30]. However, to achieve the effective hydrophilization and the water transfer of NPs, densely and chemically modified NPs are required to be synthesized [9,29,30]. Herein, we report the formation mechanism of oleic acid modified iron oxide NPs with the hydrolysis reaction in $scCO_2$, to selectively synthesize densely and chemically modified NPs with the size below 20 nm, which are important for the application. Iron(III) acetylacetonate and oleic acid of fatty acid were used as precursor and surfactant, respectively since they are highly stable and commercially available reagents [9], which makes them suitable starting materials.

2. Experimental

2.1. Materials

Iron(III) acetylacetonate [$Fe(acac)_3$] (purity over 99 %) and oleic acid (purity over 65.0 %) were purchased from Wako Pure Chemical Industries, Ltd. CO_2 (purity over 99.9 %) was supplied by Fujii Bussan Co., Ltd. Ultra-pure water was prepared using Direct-Q UV3 Water Purification System supplied by EMD Millipore Corp. and the resistivity was confirmed to be 18.2 MΩ cm.

2.2. Synthesis

Fig. 1 shows the high-pressure system to synthesize surface modified NPs in $scCO_2$. $Fe(acac)_3$ of 0.30 mmol, oleic acid of 1.50 mmol and water of 5.0–90.0 mmol were transferred to the 76 mL volume of a reaction vessel (TSC-CO_2-008; Taiatsu Glass Corp.). The molality of $Fe(acac)_3$, oleic acid and water corresponded to 0.006, 0.030 and 0.0–1.80 mol kg^{-1}, respectively, where the molality was calculated using the volume of the vessel and CO_2 density at the reaction condition. After the vessel was purged by CO_2 under 0.5 MPa for 1 min, liquified CO_2 was introduced into the vessel using a HPLC pump (PU-4386; JASCO Co., Ltd.) until reaching 6.0–7.2 MPa. After reaching the appropriate pressure, the vessel was sunk in the oil bath stirrer, which resulted in the target temperature of 100 °C and the pressure of 30.0 ± 0.9 MPa. The reaction was kept for 18 h while the enclosed materials were vigorously stirred. After the reaction, the vessel was pulled up from the oil bath stirrer and was depressurized at a rate of about 0.5 MPa min^{-1} using a metering valve (1315G2Y; HOKE Inc.). Finally, the vessel was cooled in a cyclohexane bath at room temperature.

The products were collected by rinsing the vessel successively with hexane/ethanol mixture with the volume ratio of 1:4. To remove the unreacted precursor and surfactant, the products were centrifuged and washed with the mixture of hexane and ethanol (1:4 by volume). The final precipitates were dried in a vacuum chamber at 22 °C over 18 h.

2.3. Characterization

The products were analyzed using powder X-ray diffractometer (PXRD) (MiniFlex600-C; Rigaku Corp.) with Cu Kα radiation. The products were observed using transmission electron microscope (TEM) (H-7650; Hitachi Corp.) operated at 100 kV. High resolution TEM (HR-

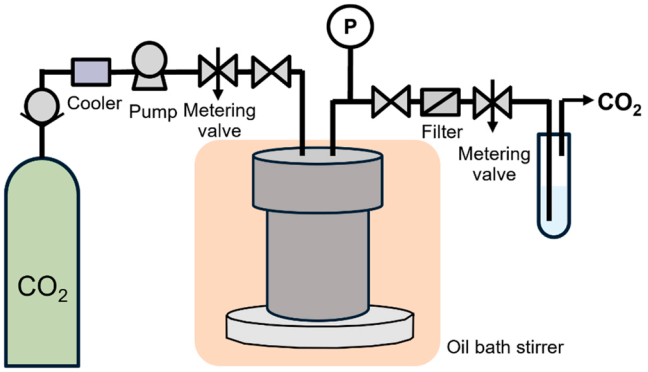

Fig. 1. Experimental equipment.

TEM) image and electron diffraction pattern of particle colony were obtained using a JEOL JEM-2010 F electron microscope operated at 200 kV. For TEM and HR-TEM analysis, the solid products were dispersed in cyclohexane and transferred onto the copper grids with organic membrane. The mean size, with their standard deviation, of the particles were determined by visually observing the contrast difference and estimating the boundary of approximately 200 particles. It was noted that attached particles with no space between them was regarded as single particle while the size of single particle was defined as a maximum length regardless of the morphologies. The products were analyzed using dynamic light scattering method (DLS) (Nano Partica SZ-100-Z: HORIBA Ltd.). The products were dispersed in toluene at the concentration of 0.01 wt % by the sonication and the dispersion was filtrated through a syringe filter (pore size: 0.2 μm) prior to the analysis. Thermogravimetric analysis was performed at N_2 atmosphere using thermogravimetric analyzer (TGA) (TGA-50; Shimadzu Corp.), where the temperature was kept at 100 °C for 20 min and was increased from 100° to 600°C at a ramp rate of 10 °C min^{-1}. The fourier transform infrared spectrometer (FT-IR) (FT-IR4100; JASCO Co., Ltd.) was used to characterize the surfactant attached to the surface of products and the surfactant attached to an iron ion.

2.4. Phase equilibrium calculation

Phase equilibrium calculations were performed to predict the phase state of synthetic field. Peng-Robison (PR) equation was used for the calculations of water + CO_2 phase equilibria and water solubility in CO_2 phase [31]. In the calculation, the below mixing rules were employed.

$$a_m = \sum_i \sum_j x_i x_j (a_i a_j)^{1/2} (1 - k_{ij}) \quad (1)$$

$$b_m = \sum_i \sum_j x_i x_j b_{ij} \quad (2)$$

$$b_{ij} = \frac{(b_i + b_j)}{2} \quad (3)$$

where α_m and b_m are the mixture's parameters. a_i and a_j are parameters reflecting attracting forces of pure components *i* and *j*. b_i and b_j are size parameters of pure component *i* and *j*. The phase composition data was acquired from the literature [32] to decide the binary interaction parameter k_{ij} and its temperature dependence. Additionally, Chrastil's equation [33], expressed as follows, was used to calculate $Fe(acac)_3$(III) and oleic acid solubility *y* to CO_2.

$$\ln y = k \ln \rho_r + \frac{m}{T} + n \quad (4)$$

where *k*, *m* and *n* are fitting parameters and ρ_r is the relative density of CO_2. The solubility data was acquired from some literatures to fit the parameters *k*, *m* and *n* for $Fe(acac)_3$(III) [13] and oleic acid [34].

3. Results and discussion

3.1. Phase state

Fitted values, summarized in Table 1, were used to calculate the solubility of starting materials in CO_2 phase at the temperature of 100 °C (Fig. 2), where each plot in Fig. 2 denotes the initial concentrations of Fe $(acac)_3$, oleic acid and water in the synthetic field. The solubilities of Fe $(acac)_3$ and oleic acid at 30.0 MPa showed significant higher values than the initial concentrations of these materials, indicating that $Fe(acac)_3$ and oleic acid were completely dissolved into $scCO_2$ at the synthesis condition (100 °C, 30.0 MPa). Whereas the water solubility in CO_2 at 30.0 MPa showed 1.20 mol kg^{-1}, suggesting that the phase separation occurs more than approximately 1.20 mol kg^{-1} of the initial water concentration.

Table 1
Fitted parameters in Eq. (1) with PR equation and in Eq. (4)

(a) Temperature dependence of binary interaction parameters in Eq. (1) with PR equation.

System	Temp. range (K)	Equation
CO_2(1) + water(2)	323 - 398	$k_{ij} = 0.5821 - 2120/T$

(b) Correlated results by Eq. (4).

System	Temp. range (K)	k	m (K)	n
CO_2(1) + $Fe(acac)_3$(2)	313 - 333	4.55	-4940	4.71
CO_2(1) + oleic acid(2)	313 - 323	7.66	-7380	12.0

3.2. Size and morphology

Fig. 3(a–f) shows the typical TEM images of products synthesized at each water amount and the size distribution histogram of product synthesized at the water amount of 5.0 mmol. Although the large amount of water (25–90 mmol) gave the severe aggregation state, the medium amount of water (10.0 mmol) gave partially aggregated state. Additionally, the small amount of water (5.0 mmol) gave the significantly reduced aggregation state of NPs with unimodal size distribution whose the mean size is 10.2 ± 2.0 nm, as shown in Fig. 3(f). These results clearly indicate that the smaller amount of water allows the synthesis of NPs with reduced aggregation state and suggest that the hydrolysis reaction is the key factor to control the size and morphology of surface modified NPs in $scCO_2$. It was noted that the irregular shaped NPs and the small aggregates of a few NPs were also observed at the condition using small amount of water, which may be due the aggregation of very small nuclei precipitated in $scCO_2$. Additionally, the DLS analysis of same product dispersed in toluene [Fig. 3(g)] showed the mean size of 88.9 ± 6.5 nm that was significantly larger than the size obtained by TEM, suggesting the formation of secondary clusters in toluene.

3.3. Crystal structure

The PXRD, TEM electron diffraction and HR-TEM analysis were performed to characterize the crystal structure of products. Fig. 4 shows the PXRD pattern of products synthesized at each water amount. The products synthesized at the large amount of water (60.0 and 90.0 mmol) gave the PXRD peaks that were assigned to α-FeOOH (ICSD: 109041) and α-Fe_2O_3 (ICSD: 22505). The products synthesized at the medium amount of water (10.0 and 25.0 mmol) gave only the peaks that were assigned to α-Fe_2O_3. The product synthesized at the small amount of water (5.0 mmol) gave very broad PXRD pattern. However, the same product showed the Debye-Scherrer ring for TEM electron diffraction analysis and the clear lattice plane for HR-TEM analysis, as shown in Fig. 5, indicating that the obtained NPs have a good crystallinity. This difference may be because of the small particle size and the low volume portion of iron oxide NPs due to the core-shell structure of iron oxide core and oleic acid shell [22]. Small particle size (corresponding to small crystallite size) typically broadens PXRD pattern. Additionally, Fig. 3(a) suggests that obtained NPs is covered with oleic acid, which is detailly discussed in chapter 3.4, enough to bring the somewhat spacing between NPs, supporting the formation of core-shell structure [1]. Assuming the core-shell structure, the volume portion of iron oxide is calculated to be 38.7 % using the core size of iron oxide (10.2 nm) and the carbon chain length of oleic acid (1.9 nm) [18]. This low volume portion causes the reduction of actual crystallite volume for PXRD measurement, which results in the decreasing intensity. Therefore, the small particle size and the low volume portion of iron oxide NPs possibly result in the broad PXRD pattern.

Table 2 lists the face spacings calculated by the electron diffraction pattern [shown in Fig. 5(a)] of obtained NPs, where each face spacing was assigned to the crystal structure of α-Fe_2O_3 (ICSD: 22505) and

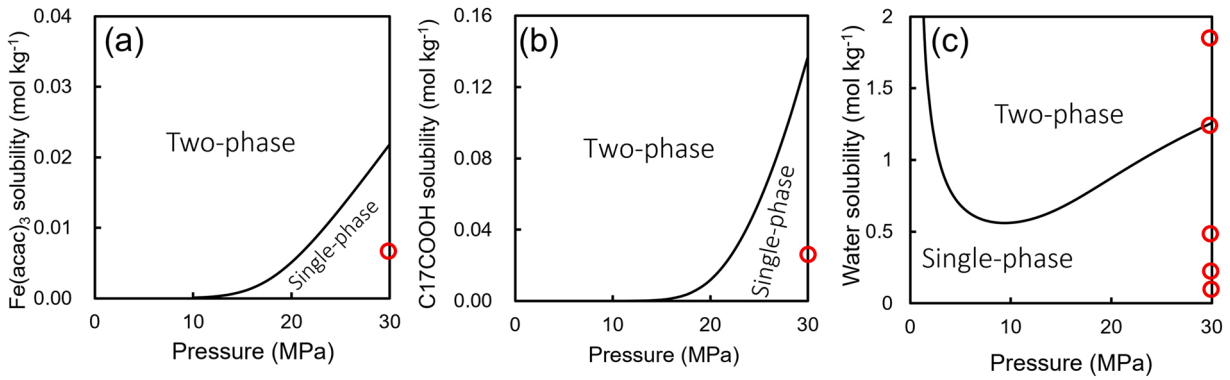

Fig. 2. The solubility (line) of (a) $Fe(acac)_3$, (b) oleic acid and (c) water in CO_2 phase at 100 °C and the initial concentration (circle) of these materials.

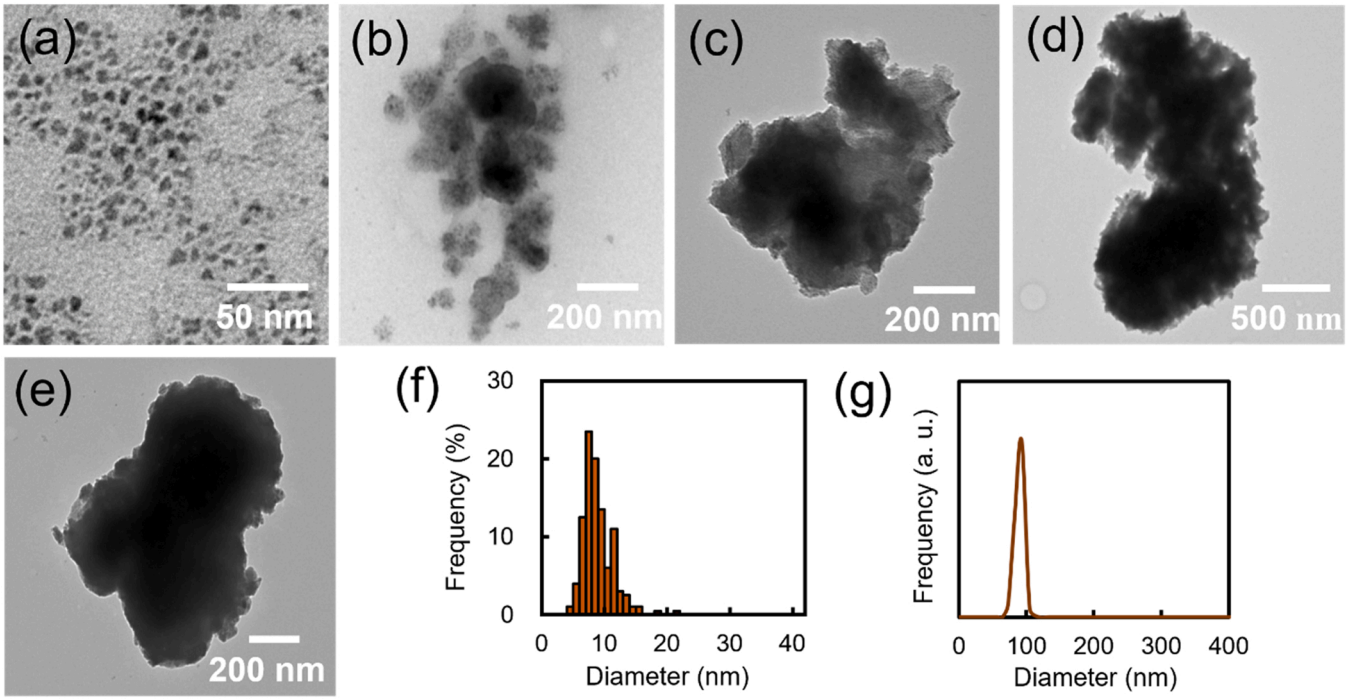

Fig. 3. (a-e) The typical TEM images of products synthesized at the water amount of (a) 5.0, (b) 10.0, (c) 25.0, (d) 60.0 and (e) 90.0 mmol. (f-g) (f) Size distribution histogram of the product synthesized at the water amount of 5.0 mmol and (g) its DLS result in toluene.

γ-Fe_2O_3 (ICSD: 79196). In short, the large amount of water (60.0–90.0 mmol) gave α-FeOOH and α-Fe_2O_3, the medium amount of water (10.0–25.0 mmol) gave α-Fe_2O_3, and the small amount of water (5.0 mmol) gave α-Fe_2O_3 and γ-Fe_2O_3. Herein, as discussed in Chapter 3.1, water phase is suggested to be separated from $scCO_2$ phase when its initial concentration is more than around 1.20 mol kg^{-1} (corresponding to the water amount of 60.0 mmol for the synthesis). Additionally, the hydrolysis reaction of iron precursor in acidic water frequently forms α-FeOOH [35]. Therefore, the reduced water amount plausibly allows the uniform reaction field without the separation of water phase, resulting in the formation of iron oxide without α-FeOOH of iron oxyhydroxide.

3.4. Surface state

The TG and FT-IR analysis were performed to characterize the oleic acid attached to the surface of NPs. Fig. 6 shows the TG spectra of products synthesized at each water amount. The weight loss showed increasing trend from 300° to 450°C that corresponded to the thermal decomposition temperature of oleic acid [21]. The total weight losses from 100° to 600°C were relatively low at the large amount of water between 25.0 and 90.0 mmol, and increased with decrease in the water amount from 25.0 to 5.0 mmol. These results suggest that the smaller amount of water leads to the formation of more densely modified NPs. Fig. 7(a–e) shows FT-IR spectra of products synthesized at each water amount. The characteristic bands at 2850 and 2900 cm^{-1} were assigned to asymmetric and symmetric stretching modes of -CH_2- in the alkyl chains of oleic acid [36]. The band of free carboxyl group (-COOH) (normally detected at 1700 cm^{-1}) in oleic acid was not confirmed in all conditions. The bands at approximately 1550 and 1400 cm^{-1} were assigned to the asymmetric and symmetric stretching modes of carboxylate group (-COO^-) in oleic acid [36]. These results evidentially show that oleic acid do not physical absorb to the surface but chemically attach to the surface of iron oxide [21]. Additionally, focusing on the relative band intensities of -CH_2- (2850 and 2900 cm^{-1}) and -COO^- (1530 and 1400 cm^{-1}), the smaller amount of water (5.0 mmol) showed significantly stronger intensities than those from the larger amount of water. Since the band intensity qualitatively reflects the amounts of molecules attached to the surface, this result further supports that the smaller amount of water leads to the formation of more densely

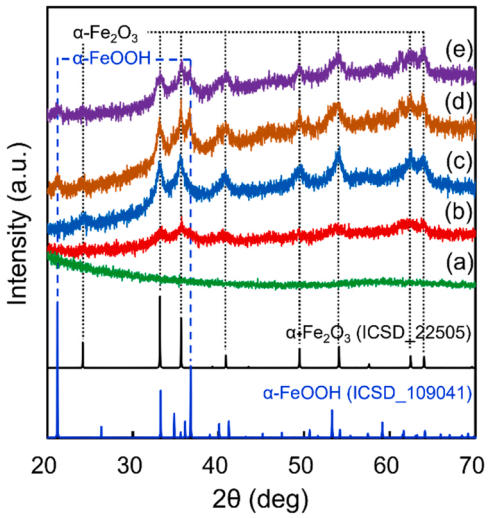

Fig. 4. The PXRD pattern of products synthesized at the water amount of (a) 5.0, (b) 10.0, (c) 25.0, (d) 60.0 and (e) 90.0 mmol.

modified NPs. Fig. 7(f) shows the enlarged FT-IR spectra of iron oxide NPs synthesized at the water amount of 5.0 mmol. The separation of asymmetric and symmetric stretching modes for -COO^-, Δ, was used to detailly analyze the chemical bonding state of oleic acid. Unidentate, bridging and bidentate ligands are expected for Δ >200 cm^{-1}, 200 cm^{-1}> Δ >140 cm^{-1} and 110 cm^{-1}> Δ, respectively [37]. For the product, two characteristic bands were confirmed at 1519 and 1430 cm^{-1}, and its difference was 89 cm^{-1}, suggesting that oleic acid is chemically bonded to the surface as a bidentate mode [20,38].

3.5. Proposed mechanism

To investigate the formation mechanism of surface modified NPs behind the effect of water amount in $scCO_2$, the synthesis was performed at 100 °C and 30.0 MPa without water addition. Fig. 8 shows the FT-IR spectra of wet solid product before aftertreatment (washing and drying). The characteristic band at 1700 cm^{-1} was assigned to -COOH of oleic acid, in addition, the bands at approximately 1550 and 1400 cm^{-1} were assigned to the asymmetric and symmetric stretching modes of -COO^- in oleic acid, respectively [36]. Herein, the thermolysis rate of $Fe(acac)_3$ is known as very small, and the calculated conversion at the reaction condition (100 °C, 18 h) was negligible based on the report from G. Beech and R. Lintonbon [39]. Additionally, the solid material could not be collected after the washing and drying, which means no particle formation without water addition. Therefore, the detected characteristic bands of -COO^- in Fig. 8(a) strongly support the formation of iron oleate complexes in $scCO_2$ without water addition. Addtionally, the key carboxylate region shows the bands at 1576, 1527 and 1431 cm^{-1}, as shown in Fig. 8(b). The defference between the band at 1431 cm^{-1} and other bands corresponded to the bridging (Δ = 145 cm^{-1}) and bidentate (Δ = 96 cm^{-1}) coordination modes of -COO^-, respectively [20,37,38]. These results suggeste that $scCO_2$ medium with oleic acid allows the formation of iron oleate complexes with these coordination modes via the ligand exchange reaction between $Fe(acac)_3$ and oleic acid.

Table 2
Face spacings and assigned structures of NPs synthesized at the water amount of 5.0 mmol.

No	Face spacing[a] (nm)	Assigned structure[b]	
1	0.242		γ-Fe_2O_3
2	0.224	α-Fe_2O_3	
3	0.208		γ-Fe_2O_3
4	0.168		γ-Fe_2O_3
5	0.149	α-Fe_2O_3	γ-Fe_2O_3

[a] Face spacings were calculated by TEM electron diffraction pattern. [b] The face spacings were assigned to the crystal structure of α-Fe_2O_3 (ICSD: 22505) and γ-Fe_2O_3 (ICSD: 79196).

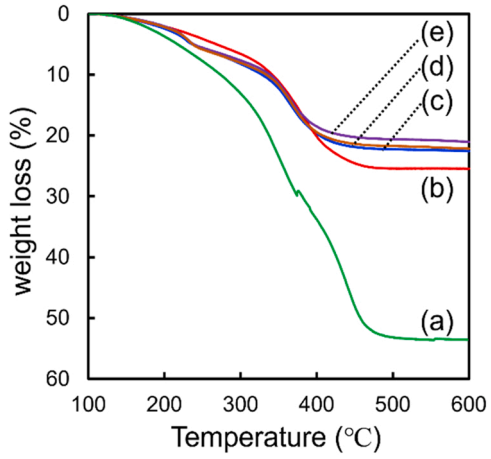

Fig. 6. TG spacetra of products synthesized at the water amount of (a) 5.0, (b) 10.0, (c) 25.0, (d) 60.0 and (e) 90.0 mmol.

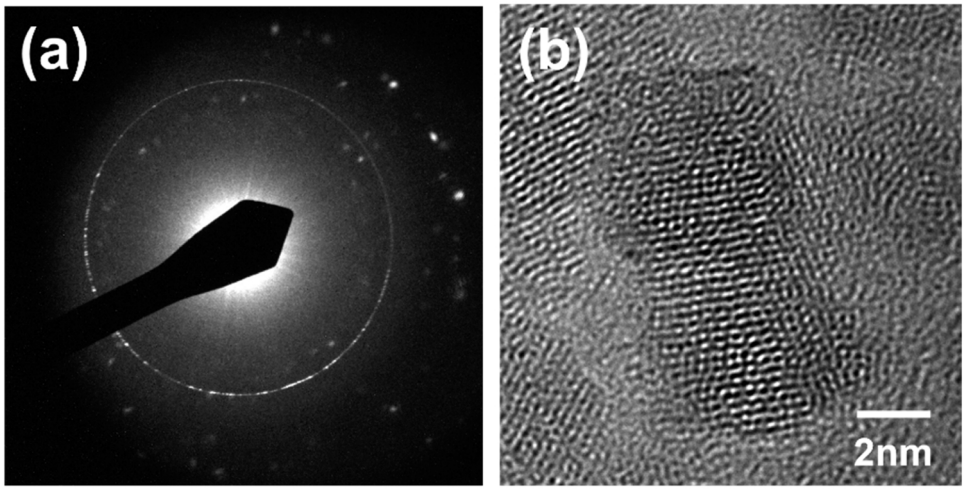

Fig. 5. (a) The electron diffraction pattern and (b) the high resolution TEM image of NPs synthesized at the water amount of 5.0 mmol.

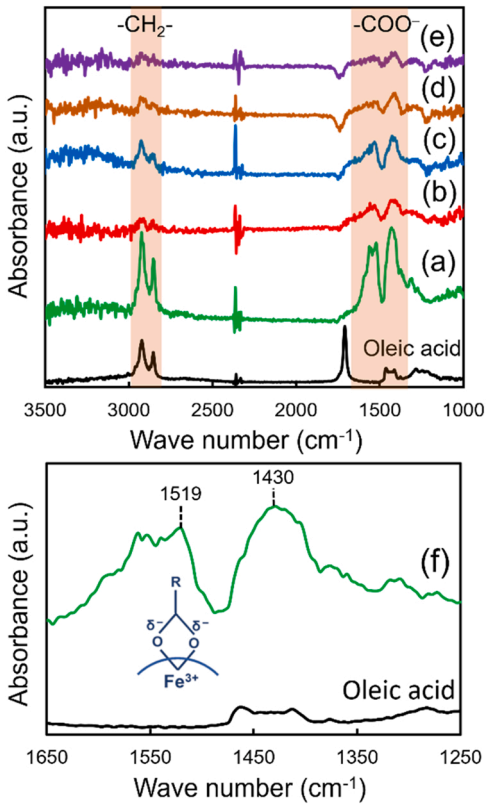

Fig. 7. (a-e) FT-IR spectra of products synthesized at the water amount of (a) 5.0, (b) 10.0, (c) 25.0, (d) 60.0, (e) 90.0 and (f) 5.0 mmol: (a-e) 1000–3500 cm^{-1} and (f) 1250–1650 cm^{-1}.

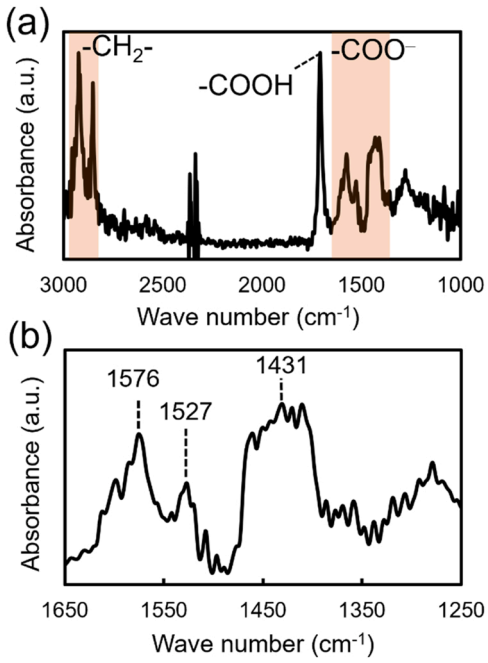

Fig. 8. FT-IR spectra of wet solid product obtained without water addition and aftertreatment (washing and drying): (a) 1000–3000 cm^{-1} and (b) 1250–1650 cm^{-1}.

The effect of water amount on the synthesis of iron oxide NPs in $scCO_2$ can be explained by the mechanism depicted in Fig. 9. The hydrolysis reaction of $Fe(acac)_3$ and subsequent particle formation are

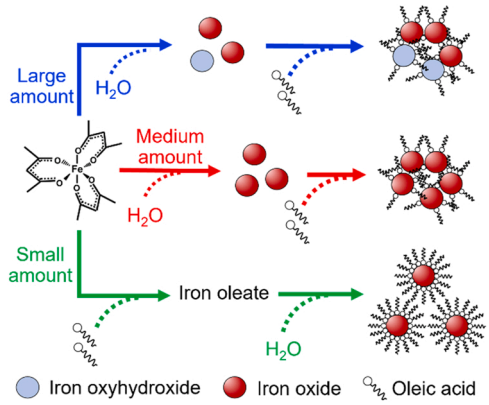

Fig. 9. Formation mechanism of surface modified NPs behind the effect of water amount in $scCO_2$.

confirmed in our previous research with the same reaction condition (100 °C, 30.0 MPa) [22] and iron oleate formation is validated by the analysis in previous paragraph, which supports that the hydrolysis of Fe $(acac)_3$ competes the iron oleate formation. When the large or medium amount of water exist in $scCO_2$, the hydrolysis of $Fe(acac)_3$ should be faster than the iron oleate formation, resulting in the nucleation of less modified NPs. Such iron oxide NPs typically has hydrophilic surface that is low compatible to $scCO_2$ with nonpolar property and causes the low steric hindrance between NPs, which easily leads to the severe aggregation of less modified NPs (Fig. 9). Since the aggregated NPs are not easily disaggregated and additionally modified, the final product reflects the less modified surface, resulting in the relatively small weight loss and band intensities assigned to oleic acid for TG and FT-IR analysis, respectively. Additionally, the large amount of water above the solubility causes the phase separation of water, resulting in the formation of iron oxyhydroxide (Fig. 9). In contrast to them, the small amount of water allows the uniform reaction field and the relatively faster formation of iron oleate than the hydrolysis reaction of $Fe(acac)_3$. As a result, iron oxide NPs is synthesized through the hydrolysis reaction of iron oleate complexes (Fig. 9). As widely known in hydrothermal method [5,6,18], the hydrolysis reaction of iron oleate leads to the nucleation of chemically and densely modified iron oxide NPs. Such NPs induces the strong steric hindrance between NPs and has the hydrophobic surface that is compatible with $scCO_2$, which inhibits the aggregation. Therefore, it can be concluded that the smaller amount of water allows more dominated formation of iron oleate and subsequent its hydrolysis reaction in uniform $scCO_2$ phase, resulting in the formation of densely and chemically modified iron oxide NPs without the aggregation.

4. Conclusions

In this study, surface modified iron oxide NPs was synthesized in $scCO_2$ with various amounts of water to reveal the formation mechanism of surface modified NPs with the hydrolysis reaction. The synthesis was performed at 30.0 ± 0.9 MPa of CO_2 and 100 °C for 18 h, where iron(III) acetylacetonate of 0.30 mmol (0.006 mol kg^{-1}), oleic acid of 1.50 mmol (0.030 mol kg^{-1}) and water of 0.0–90.0 mmol (0.0–1.80 mol kg^{-1}) were used as starting materials. TEM and XRD analysis revealed that the smaller amount of water led to the formation of iron oxide NPs without the aggregation as opposed to the aggregated NPs for the larger amount of water. Additionally, TG and FT-IR analysis supported that the smaller amount of water led to the formation of more densely modified NPs than those from the larger amount of water. These results suggest that the smaller amount of water is crucial to synthesize densely modified NPs, resulting in the inhibition of the aggregation. Additionally, the detailed analysis of iron oleate complex and the phase state prediction of synthetic field suggested that the smaller amount of water allowed more

dominated formation of iron oleate and subsequent its hydrolysis reaction in uniform $scCO_2$ phase, resulting in the formation of densely and chemically modified NPs without the aggregation. These findings are important and useful to design surface modified NPs using the hydrolysis reaction in $scCO_2$, contributing to the development of green chemistry approach based on the utilization of water and CO_2.

CRediT authorship contribution statement

Yasuhiko Orita: Conceptualization, Methodology, Investigation, Resources, Writing – original draft, Visualization, Supervision, Project administration, Funding acquisition. **Keito Kariya**: Methodology, Validation, Investigation, Visualization. **Thossaporn Wijakmatee**: Methodology, Investigation. **Yusuke Shimoyama**: Resources, Writing – review & editing, Project administration.

Declaration of Competing Interest

The authors declare that they have no known competing financial interests or personal relationships that could have appeared to influence the work reported in this paper.

Data availability

The data that has been used is confidential.

Acknowledgements

This work was supported by the Japan Society for the Promotion of Science, Grant-in-Aid for Early-Career Scientists JP21K14454. This work was supported by Futaba Foundation (The Futaba Research Grant Program) in Japan. This work was supported by Shorai Foundation for Science and Technology in Japan. This work was supported by Tokuyama Science Foundation in Japan.

References

[1] T. Tomai, N. Tajima, M. Kimura, A. Yoko, G. Seong, T. Adschiri, Solvent accommodation effect on dispersibility of metal oxide nanoparticle with chemisorbed organic shell, J. Colloid Interface Sci. 587 (2021) 574–580, https://doi.org/10.1016/j.jcis.2020.11.014.

[2] G. Zhao, J.J. Xu, H.Y. Chen, Fabrication, characterization of Fe_3O_4 multilayer film and its application in promoting direct electron transfer of hemoglobin, Electrochem. Commun. 8 (2006) 148–154, https://doi.org/10.1016/j.elecom.2005.11.001.

[3] T. Teranishi, A. Sugawara, T. Shimizu, M. Miyake, Planar array of 1D gold nanoparticles on ridge-and-valley structured carbon, J. Am. Chem. Soc. 124 (2002) 4210–4211, https://doi.org/10.1021/ja017536k.

[4] L. Shen, B. Li, Y. Qiao, Fe_3O_4 nanoparticles in targeted drug/gene delivery systems, Materials 11 (2018) 1–29, https://doi.org/10.3390/ma11020324.

[5] Y.V. Kolen'Ko, M. Bañobre-López, C. Rodríguez-Abreu, E. Carbó-Argibay, A. Sailsman, Y. Piñeiro-Redondo, M.F. Cerqueira, D.Y. Petrovykh, K. Kovnir, O. I. Lebedev, J. Rivas, Large-scale synthesis of colloidal Fe_3O_4 nanoparticles exhibiting high heating efficiency in magnetic hyperthermia, J. Phys. Chem. C 118 (2014) 8691–8701, https://doi.org/10.1021/jp500816u.

[6] T. Taniguchi, K. Nakagawa, T. Watanabe, N. Matsushita, M. Yoshimura, Hydrothermal growth of fatty acid stabilized iron oxide nanocrystals, J. Phys. Chem. C 113 (2009) 839–843, https://doi.org/10.1021/jp8062433.

[7] F. Ansari, A. Sobhani, M. Salavati-Niasari, Simple sol-gel synthesis and characterization of new $CoTiO_3$/$CoFe_2O_4$ nanocomposite by using liquid glucose, maltose and starch as fuel, capping and reducing agents, J. Colloid Interface Sci. 514 (2018) 723–732, https://doi.org/10.1016/j.jcis.2017.12.083.

[8] C.B. Murray, C.R. Kagan, M.G. Bawendi, Synthesis and characterization of monodisperse nanocrystals and close-packed nanocrystal assemblies, Annu. Rev. Mater. Sci. 30 (2000) 545–610, https://doi.org/10.1146/annurev.matsci.30.1.545.

[9] J. Muro-Cruces, A.G. Roca, A. López-Ortega, E. Fantechi, D. Del-Pozo-Bueno, S. Estradé, F. Peiró, B. Sepúlveda, F. Pineider, C. Sangregorio, J. Nogues, Precise size control of the growth of Fe_3O_4 nanocubes over a wide size range using a rationally designed one-pot synthesis, ACS Nano (2019) 7716–7728, https://doi.org/10.1021/acsnano.9b01281.

[10] J. Zhang, S. Ohara, M. Umetsu, T. Naka, Y. Hatakeyama, T. Adschiri, Colloidal ceria nanocrystals: a tailor-made crystal morphology in supercritical water, Adv. Mater. 19 (2007) 203–206, https://doi.org/10.1002/adma.200600964.

[11] M. Kinoshita, T. Kamizato, Y. Shimoyama, Effect of precursor structure on mixed-crystal phase titanium oxide synthesized by sol-gel reaction in supercritical carbon dioxide, J. Supercrit. Fluids 138 (2018) 193–199, https://doi.org/10.1016/j.supflu.2018.04.017.

[12] M. Kinoshita, Y. Shimoyama, Dynamic phase behavior during sol-gel reaction in supercritical carbon dioxide for morphological design of nanostructured titania, J. Supercrit. Fluids 116 (2016) 190–197, https://doi.org/10.1016/j.supflu.2016.05.008.

[13] M. Haruki, F. Kobayashi, S.I. Kihara, S. Takishima, Effect of the chemical structures of iron complexes on the solubilities in supercritical carbon dioxide, Fluid Phase Equilib. 308 (2011) 1–7, https://doi.org/10.1016/j.fluid.2011.05.008.

[14] E. Alonso, I. Montequi, S. Lucas, M.J. Cocero, Synthesis of titanium oxide particles in supercritical CO_2: effect of operational variables in the characteristics of the final product, J. Supercrit. Fluids 39 (2007) 453–461, https://doi.org/10.1016/j.supflu.2006.03.006.

[15] X. Dong, D. Potter, C. Erkey, Synthesis of CuS nanoparticles in water-in-carbon dioxide microemulsions, Ind. Eng. Chem. Res. 41 (2002) 4489–4493, https://doi.org/10.1021/ie0107892.

[16] S.W. Kim, J.P. Ahn, Polycrystalline nanowires of gadolinium-doped ceria via random alignment mediated by supercritical carbon dioxide, Sci. Rep. 3 (2013) 3–7, https://doi.org/10.1038/srep01606.

[17] S.H. Wang, J.H. Liu, C.T. Pai, C.W. Chen, P.T. Chung, A.S.T. Chiang, S.J. Chang, Hansen solubility parameter analysis on the dispersion of zirconia nanocrystals, J. Colloid Interface Sci. 407 (2013) 140–147, https://doi.org/10.1016/j.jcis.2013.07.001.

[18] T. Adschiri, S. Takami, T. Arita, D. Hojo, K. Minami, N. Aoki, T. Togashi, Supercritical Hydrothermal Synthesis. Handbook Adv. Ceramics: Mater. Appl. Processing Properties, 2th ed., Elsevier, 2013, pp. 949–978, https://doi.org/10.1016/B978-0-12-385469-8.00051-4.

[19] E. Scopel, P.P. Conti, D.G. Stroppa, C.J. Dalmaschio, Synthesis of functionalized magnetite nanoparticles using only oleic acid and iron (III) acetylacetonate, SN Appl. Sci. 1 (2019) 1–8, https://doi.org/10.1007/s42452-018-0140-6.

[20] S.J. Kemp, R.M. Ferguson, A.P. Khandhar, K.M. Krishnan, Monodisperse magnetite nanoparticles with nearly ideal saturation magnetization, RSC Adv. 6 (2016) 77452–77464, https://doi.org/10.1039/c6ra12072e.

[21] M. Taguchi, N. Yamamoto, D. Hojo, S. Takami, T. Adschiri, T. Funazukuri, T. Naka, Synthesis of monocarboxylic acid-modified CeO_2 nanoparticles using supercritical water, RSC Adv. 4 (2014) 49605–49613, https://doi.org/10.1039/c4ra06936f.

[22] Y. Orita, K. Kariya, T. Wijakmatee, Y. Shimoyama, Synthesis of surface-modified iron oxide nanocrystals using supercritical carbon dioxide as the reaction field, RSC Adv. 12 (2022) 7990–7995, https://doi.org/10.1039/d1ra08580h.

[23] D. Bobo, K.J. Robinson, J. Islam, K.J. Thurecht, S.R. Corrie, Nanoparticle-based medicines: A review of FDA-approved materials and clinical trials to date, Pharm. Res. 33 (2016) 2373–2387, https://doi.org/10.1007/s11095-016-1958-5.

[24] H. Li, Y.J. Zhu, Liquid-phase synthesis of iron oxide nanostructured materials and their applications, Chem. - A Eur. J. 26 (2020) 9180–9205, https://doi.org/10.1002/chem.202000679.

[25] S.Arora Wahajuddin, Superparamagnetic iron oxide nanoparticles: magnetic nanoplatforms as drug carriers, Int. J. Nanomed. 7 (2012) 3445–3471, https://doi.org/10.2147/IJN.S30320.

[26] L.T.H. Phong, D.H. Manh, P.H. Nam, V.D. Lam, B.X. Khuyen, B.S. Tung, T.N. Bach, D.K. Tung, N.X. Phuc, T.V. Hung, T.L. Mai, T.L. Phan, M.H. Phan, Structural, magnetic and hyperthermia properties and their correlation in cobalt-doped magnetite nanoparticles, RSC Adv. 12 (2021) 698–707, https://doi.org/10.1039/d1ra07407e.

[27] Y. Tian, B. Yu, X. Li, K. Li, Facile solvothermal synthesis of monodisperse Fe_3O_4 nanocrystals with precise size control of one nanometre as potential MRI contrast agents, J. Mater. Chem. 21 (2011) 2476–2481, https://doi.org/10.1039/c0jm02913k.

[28] K. Lind, M. Kresse, N.P. Debus, R.H. Müller, A novel formulation for superparamagnetic iron oxide (SPIO) particles enhancing MR lymphography: comparison of physicochemical properties and the in vivo behaviour, J. Drug Target 10 (2002) 221–230, https://doi.org/10.1080/10611860290022651.

[29] J. Zhang, R.D.K. Misra, Magnetic drug-targeting carrier encapsulated with thermosensitive smart polymer: core-shell nanoparticle carrier and drug release response, Acta Biomater. 3 (2007) 838–850, https://doi.org/10.1016/j.actbio.2007.05.011.

[30] X. Yang, H. Hong, J.J. Grailer, I.J. Rowland, A. Javadi, S.A. Hurley, Y. Xiao, Y. Yang, Y. Zhang, R.J. Nickles, W. Cai, D.A. Steeber, S. Gong, cRGD-functionalized, DOX-conjugated, and 64Cu-labeled superparamagnetic iron oxide nanoparticles for targeted anticancer drug delivery and PET/MR imaging, Biomaterials 32 (2011) 4151–4160, https://doi.org/10.1016/j.biomaterials.2011.02.006.

[31] D. Peng, D.B. Robinson, A new two-constant equation of state, Ind. Eng. Chem. Fundamen. 15 (1976) 59–64, https://doi.org/10.1021/i160057a011.

[32] S.X. Hou, G.C. Maitland, J.P.M. Trusler, Measurement and modeling of the phase behavior of the (carbon dioxide + water) mixture at temperatures from 298.15 K to 448.15 K, J. Supercrit. Fluids 73 (2013) 87–96, https://doi.org/10.1016/j.supflu.2012.11.011.

[33] J. Chrastil, Solubility of solids and liquids in supercritical gases, J. Phys. Chem. 86 (1982) 3016–3021, https://doi.org/10.1021/j100212a041.

[34] M. Skerget, Z. Knez, M. Habulin, Solubility of β-carotene and oleic acid in dense CO_2 and data correlation by a density based model, Fluid Phase Equilb. 109 (1995) 131–138, https://doi.org/10.1016/0378-3812(95)02717-S.

[35] M.K. Sinha, S.K. Sahu, P. Meshram, L.B. Prasad, B.D. Pandey, Low temperature hydrothermal synthesis and characterization of iron oxide powders of diverse morphologies from spent pickle liquor, Powder Technol. 276 (2015) 214–221, https://doi.org/10.1016/j.powtec.2015.02.006.

[36] K. Nakanishi, Structural Information: Infrared Absorption Spectroscopy: Practical, Holden-Day, San Francisco, 1962, p. 223, https://doi.org/10.1126/science.140.3567.648.a.
[37] K. Nakamoto. Infrared and Raman Spectra of Inorganic and Coordination Compounds, 5th ed.,, Wiley, New York, 1997, p. 387.
[38] L.M. Bronstein, X. Huang, J. Retrum, A. Schmucker, M. Pink, B.D. Stein, B. Dragnea, Influence of iron oleate complex structure on iron oxide nanoparticle formation, Chem. Mater. 19 (2007) 3624–3632, https://doi.org/10.1021/cm062948j.
[39] G. Beech, R. Lintonbon, Thermal and kinetic studies of some complexes of 2,4-pentanedione, Thermochim. Acta 3 (1971) 97–105, https://doi.org/10.1016/0040-6031(71)80003-5.